

# THE DISTRIBUTION, EXCITATION AND FORMATION OF COMETARY MOLECULES: METHANOL, METHYL CYANIDE AND ETHYLENE GLYCOL

Anthony J. Remijan<sup>1</sup>, Stefanie N. Milam<sup>2,3</sup>, Maria Womack<sup>4</sup>, A. J. Apponi<sup>2</sup>, L. M. Ziurys<sup>2</sup>, Susan Wyckoff<sup>5</sup>, M. F. A'Hearn<sup>6</sup>, Imke de Pater<sup>7</sup>, J. R. Forster<sup>7</sup>, D. N. Friedel<sup>8</sup>, Patrick Palmer<sup>9</sup>, L. E. Snyder<sup>8</sup>, J. M. Veal<sup>8,10</sup>, L. M. Woodney<sup>11</sup>, & M. C. H. Wright<sup>7</sup>

## ABSTRACT

We present an interferometric and single dish study of small organic species toward Comets C/1995 O1 (Hale-Bopp) and C/2002 T7 (LINEAR) using the BIMA interferometer at 3 mm and the ARO 12m telescope at 2 mm. For Comet Hale-Bopp, both the single-dish and interferometer observations of CH<sub>3</sub>OH indicate an excitation temperature of  $105 \pm 5$  K and an average production rate ratio

---

<sup>1</sup>National Radio Astronomy Observatory, 520 Edgemont Road, Charlottesville, VA 22901  
email: aremijan@nrao.edu.

<sup>2</sup>NASA Astrobiology Institute, Department of Chemistry, Department of Astronomy, and Steward Observatory, 933 North Cherry Avenue, University of Arizona, Tucson, AZ 85721; email: lziurys@as.arizona.edu, aapponi@as.arizona.edu.

<sup>3</sup>Current Address: NASA Ames Research Center, Astrophysics Branch MS 245-6, Moffett Field, CA 94035-1000; email: stefanie.n.milam@nasa.gov

<sup>4</sup>Department of Physics and Astronomy, St. Cloud State University, St. Cloud, MN 56301; mwomack@stcloudstate.edu.

<sup>5</sup>Department of Physics and Astronomy, Arizona State University, Tempe AZ 85287; wyckoff@asu.edu.

<sup>6</sup>Department of Astronomy, University of Maryland, College Park MD 20742-2421 email: ma@astro.umd.edu

<sup>7</sup>Department of Astronomy, University of California, Berkeley, CA 94720 email: imke@floris.berkeley.edu, rforster@astro.berkeley.edu, wright@astro.berkeley.edu

<sup>8</sup>Department of Astronomy, 1002 W. Green St., University of Illinois, Urbana IL 61801 email: friedel@astro.uiuc.edu, snyder@astro.uiuc.edu

<sup>9</sup>Department of Astronomy and Astrophysics, University of Chicago, Chicago, IL 60637 email: ppalmer@oskar.uchicago.edu

<sup>10</sup>Current address: Southwestern College, 900 Otay Lakes Road, Chula Vista, CA 91910; jveal@swccd.edu

<sup>11</sup>Department of Physics, California State University, San Bernardino, CA 92407; woodney@csusb.edu.

$Q(\text{CH}_3\text{OH})/Q(\text{H}_2\text{O}) \sim 1.3\%$  at  $\sim 1$  AU. Additionally, the aperture synthesis observations of  $\text{CH}_3\text{OH}$  suggest a distribution well described by a spherical outflow and no evidence of significant extended emission. Single-dish observations of  $\text{CH}_3\text{CN}$  in Comet Hale-Bopp indicate an excitation temperature of  $200 \pm 10$  K and a production rate ratio of  $Q(\text{CH}_3\text{CN})/Q(\text{H}_2\text{O}) \sim 0.017\%$  at  $\sim 1$  AU. The non-detection of a previously claimed transition of cometary  $(\text{CH}_2\text{OH})_2$  toward Comet Hale-Bopp with the 12m telescope indicates a compact distribution of emission,  $D < 9''$  ( $< 8500$  km). For the single-dish observations of Comet T7 LINEAR, we find an excitation temperature of  $\text{CH}_3\text{OH}$  of  $35 \pm 5$  K and a  $\text{CH}_3\text{OH}$  production rate ratio of  $Q(\text{CH}_3\text{OH})/Q(\text{H}_2\text{O}) \sim 1.5\%$  at  $\sim 0.3$  AU. Our data support current chemical models that  $\text{CH}_3\text{OH}$ ,  $\text{CH}_3\text{CN}$  and  $(\text{CH}_2\text{OH})_2$  are parent nuclear species distributed into the coma via direct sublimation off cometary ices from the nucleus with no evidence of significant production in the outer coma.

*Subject headings:* astrobiology - comets: individual (HALE BOPP (C/1995 01), LINEAR (C/2002 T7)) - molecular processes - techniques: interferometric - radio lines: solar system

## 1. INTRODUCTION

Over the last several years, complementary observations of comets with both single-dish telescopes and interferometric arrays, have shed new light on the abundance, production rate, distribution and formation of molecules in cometary comae. Recently, Milam et al. (2006) employed this method to investigate the origins of cometary formaldehyde ( $\text{H}_2\text{CO}$ ) by comparing observations with both the Arizona Radio Observatory (ARO) 12m<sup>12</sup> single-dish telescope and the Berkeley-Illinois-Maryland Association (BIMA) array<sup>13</sup>. From this investigation toward Comet C/1995 O1 (Hale-Bopp), the authors clearly showed that the distribution and abundance of  $\text{H}_2\text{CO}$  must be coming from a source other than the comet nucleus. The extended source of  $\text{H}_2\text{CO}$  may be due to an enhanced production of this molecule, ( $\sim 4 \times$  larger) from grains consisting of silicates and organic material (Milam et al. 2006), or possibly from the photodissociation of a larger parent species such as methanol ( $\text{CH}_3\text{OH}$ ) (Hudson, Moore & Cook 2005). These complementary observations, however, are very dif-

---

<sup>12</sup>The Kitt Peak 12m telescope is currently operated by Arizona Radio Observatory (ARO), Steward Observatory, University of Arizona.

<sup>13</sup>Operated by the University of California, Berkeley, the University of Illinois, and the University of Maryland with support from the National Science Foundation.

difficult to obtain, as most of the molecular observations toward comets are performed using solely single-dish telescopes or interferometric arrays, depending on the telescope available at the time as the comet approaches the inner solar system and perigee.

Multiple facility collaborations for cometary observations are necessary if we are to further understand the formation, excitation and distribution of organic cometary material. Recent cometary models of the abundance of organic material suggest Oort Cloud comets may have had an origin in the giant planet region, where they were thermally and chemically processed, before being ejected into the Oort Cloud (Weissman 1999). Furthermore, observations comparing long- and short-period comets suggest distinct classes - organic “rich”, “normal”, and “depleted” (Bonev et al. 2008; Mumma et al. 2003). However, the current sample size is too limited to accurately characterize each class of comets. It should also be noted that many of the comets described as organic “rich” have undergone breakup or fragmentation events, thus exposing more internal, unprocessed material than an object just entering the inner solar system (Bonev et al. 2008). So, the question persists, how does the classification of organic “rich”, “normal” or “depleted” hold with regards to comets that are for example, dust rich versus dust poor, having undergone a recent breakup, or bear high abundances of hypervolatile species?

The organic species examined in this study, methanol ( $\text{CH}_3\text{OH}$ ), methyl cyanide ( $\text{CH}_3\text{CN}$ ) and ethylene glycol ( $[\text{CH}_2\text{OH}]_2$ ) are believed to be parent species directly sublimated off the cometary ices in the nucleus. Since the first reported single-dish detections of cometary  $\text{CH}_3\text{OH}$  towards Comet Brorsen-Metcalf (1989 o) and Comet Austin (1989 c1) (Colom et al. 1990),  $\text{CH}_3\text{OH}$  remains the most abundant large ( $>5$  atoms) organic (containing a C-atom) molecule measured in cometary ices. In a recent review by Charnley & Rodgers (2008),  $\text{CH}_3\text{OH}$  has a measured abundance range relative to  $\text{H}_2\text{O}$  between 1-4%. However, aperture synthesis observations of cometary  $\text{CH}_3\text{OH}$  are very rare and no high spatial resolution data of this molecule currently exists. Similarly, single-dish observations of  $\text{CH}_3\text{CN}$  and  $(\text{CH}_2\text{OH})_2$  also suggest a purely nuclear origin (Biver et al. 2002, Crovisier et al. 2004).  $\text{CH}_3\text{CN}$ , as well as  $\text{HC}_3\text{N}$ , may be parent species that would increase the abundance of the CN radical as well as  $\text{C}_2$  in the coma. Yet, current observations do not preclude the possibility of  $\text{CH}_3\text{CN}$  having its own parent species (Bockelée-Morvan et al. 1987). In addition, the high abundance of  $(\text{CH}_2\text{OH})_2$  observed in Comet Hale-Bopp at high spatial resolution also strongly suggests a nuclear origin. To date, complementary observations of the same transitions of either  $\text{CH}_3\text{CN}$  or  $(\text{CH}_2\text{OH})_2$  with another facility were not available to follow-up on the claimed distribution of these species in the coma and their possible formation pathways.

In this paper, we report on complementary observations of cometary  $\text{CH}_3\text{OH}$ ,  $\text{CH}_3\text{CN}$  and  $(\text{CH}_2\text{OH})_2$  taken with the BIMA array near Hat Creek, CA and the ARO 12m telescope

on Kitt Peak, AZ toward Comets C/1995 O1 (Hale-Bopp) and C/2002 T7 (LINEAR). From these observations, we continued to investigate the abundance, production rate, distribution and formation of molecules in comets by directly comparing the measurements of these organic species with different telescopes. Our data supports the hypothesis that  $\text{CH}_3\text{OH}$ ,  $\text{CH}_3\text{CN}$  and  $(\text{CH}_2\text{OH})_2$  are primarily parent species, generated by direct sublimation of cometary ices contained in the nucleus.

## 2. OBSERVATIONS

### 2.1. BIMA Array

Our observations of Comet Hale-Bopp with the BIMA array constitute one of the earliest detections of cometary  $\text{CH}_3\text{OH}$  with an interferometer. These measurements were taken using the “soft” C configuration of the BIMA array from 1997 March 24 to April 03. Data were acquired in the interferometric (cross-correlation) mode with nine antennas. The minimum baseline for these observations was  $\sim 15$  m and the maximum baseline was  $\sim 139$  m. The average resulting full width half power synthesized beam size was  $\sim 8'' \times 10''$  for the observations. The quasar 0102+584 was used to calibrate the antenna based gains and the absolute amplitude calibration of this source was based on planetary observations and is accurate to within  $\sim 20\%$ . The spectral windows containing the transitions had a bandwidth of 25 MHz and were divided into 256 channels for a spectral resolution of 0.1 MHz per channel. However, to increase the signal-to-noise ratio in each window, the data were averaged over two channels giving an effective spectral resolution of 0.2 MHz per channel. All data were first corrected to JPL ephemeris reference orbit 139. The data were then combined and imaged using the MIRIAD software package (Sault, Teuben & Wright 1995). To include all the data from the comet with multiple tracks, the data were inverted in  $u$ - $v$  space. The resulting synthesized beamsizes were determined from the combined dataset. The uvdata from multiple tracks were combined to make images. Table 1 summarizes the observational parameters of the BIMA array observations.

### 2.2. 12m Single Dish

Observations at 2mm of  $\text{CH}_3\text{OH}$ ,  $\text{CH}_3\text{CN}$  and  $(\text{CH}_2\text{OH})_2$  toward Comet Hale-Bopp were taken during three observing runs on 1997 Mar 10, 11, and 20 using the ARO (at

the time, NRAO<sup>14</sup>) 12m telescope. Observations of CH<sub>3</sub>OH toward Comet LINEAR were conducted on 2004 May 20 also using the ARO 12m telescope. Dual-channel SIS mixers were used for the 2 mm observations, operated in single-sideband mode with  $\sim 20$  dB image rejection. The backends employed for the presented observations were individual filter banks with 500 kHz resolution and the millimeter autocorrelator (MAC) with a resolution of 781 kHz. The spectral temperature scale was determined by the chopper-wheel method, corrected for forward spillover losses, given in terms of  $T_R^*$  (K). The radiation temperature,  $T_R$ , is then derived from the corrected beam efficiency,  $\eta_c$ , where  $T_R = T_R^*/\eta_c$ . A two body ephemeris program was used to determine the comet’s position using the orbital elements provided by D. Yeomans (1996, private communication) of JPL for Comet Hale-Bopp and JPL ephemeris reference orbit 69 was used for the Comet LINEAR observations. Focus and positional accuracy were checked periodically on nearby planets or maser sources. Data were taken in the position-switched mode with the off position 30’ west in azimuth. Observing frequencies, dates, comet geocentric and heliocentric distances, beam size, the diameter of the projected beam size on the comet, and the corrected main beam efficiency ( $\eta_c$ ) at the times of observations are listed in Table 2.

Table 3 lists the transitions and molecular line parameters of CH<sub>3</sub>OH, CH<sub>3</sub>CN and (CH<sub>2</sub>OH)<sub>2</sub>. All spectral line data were taken from the Spectral Line Atlas of Interstellar Molecules (SLAIM) available at [www.splatalogue.net](http://www.splatalogue.net) (Remijan et al. 2008) and the Cologne Database for Molecular Spectroscopy (Müller et al. 2005).

### 3. RESULTS

#### 3.1. BIMA Array

Figure 1 shows the images and spectra of CH<sub>3</sub>OH taken toward Comet Hale-Bopp with the BIMA array. Figure 1(a) shows the image of the J(K<sub>a</sub>,K<sub>c</sub>)=2(0,2)-1(0,1) E transition of CH<sub>3</sub>OH averaged over 2 days, 1997 March 27 and 31. Notice that the CH<sub>3</sub>OH emission is slightly larger than the synthesized beam of the BIMA array (located at the bottom left of each image) and follows the general position angle of the synthesized beam. The projected direction to the sun is shown by the line segment. The coordinates are given in offset arcseconds centered on the comet nucleus. Figure 1(b) shows the spectra of 4 CH<sub>3</sub>OH transitions near 96.7 GHz (Table 3) including the J(K<sub>a</sub>,K<sub>c</sub>)=2(0,2)-1(0,1) E transition. The

---

<sup>14</sup>The National Radio Astronomy Observatory is a facility of the National Science Foundation operated under cooperative agreement by the Associated Universities, Inc.

spectrum has been hanning smoothed over 3 channels. The rms noise level is  $\sim 0.1 \text{ Jy beam}^{-1}$  (indicated by the vertical bar at the left of the spectrum). The spectral line labels correspond to the rest frequency located at the top left of the panel for a cometocentric velocity of  $0 \text{ km s}^{-1}$ , denoted by a dashed line.

Figure 1(c) shows the image of the  $J(K_a, K_c)=3(1,3)-4(0,4) \text{ A}^+$  transition of  $\text{CH}_3\text{OH}$  averaged over 3 days, 1997 March 26 and April 2-3. Figure 1(d) shows the spectrum of this  $\text{CH}_3\text{OH}$  transition near 107.0 GHz (Table 3). Note that the two  $\text{CH}_3\text{OH}$  emission contours shown in figures (a) and (c) are centered on the predicted location of the comet nucleus with no apparent offset. The images are similar to each other and similar to the average of the March HCN BIMA array contours given by Veal et al. (2000) and the CO BIMA array contours given by Milam et al. (2006). In addition, there is no pronounced evidence for the jets or significant extended enhancement of  $\text{CH}_3\text{OH}$  beyond the  $3\sigma$  detection level (§4.2). Furthermore, from figures 1(b) and (d), there is no apparent second velocity component of  $\text{CH}_3\text{OH}$  nor is the emission offset from the cometocentric rest velocity of  $0 \text{ km s}^{-1}$ .

### 3.2. 12m Single Dish

Figure 2 shows the spectra of the five  $\lambda \simeq 2\text{mm}$  transitions of  $\text{CH}_3\text{OH}$  detected toward Comet Hale-Bopp with the 12m telescope (Table 3). The UT date and spectral line quantum numbers of each observed transition are located at the top of each panel. As in the BIMA spectra, the spectral line labels correspond to the rest frequency of that transition for a cometocentric velocity of  $0 \text{ km s}^{-1}$  (dashed line). The  $\text{CH}_3\text{OH}$  detections reported by the 12m data are all E-type transitions. Similarly, Figure 3 shows the spectrum of a cluster of E-type transitions of  $\text{CH}_3\text{OH}$  centered around 157.3 GHz observed toward Comet LINEAR with the ARO 12m telescope.

Finally, Figure 4 shows the spectrum taken at the frequency of the  $J = 8 - 7$  ( $K=0$  through 7) transitions of the symmetric top species methyl cyanide ( $\text{CH}_3\text{CN}$ ) toward Comet Hale-Bopp using the 12m. The  $K=0$  through 6 components are clearly present in these data.  $\text{CH}_3\text{CN}$  and other symmetric tops have properties that make them ideal probes of physical conditions of astronomical environments (see e.g. Araya et al. 2005; Remijan et al. 2004; Hofner et al. 1996 ). As with  $\text{CH}_3\text{OH}$ , there is no apparent additional velocity components of  $\text{CH}_3\text{CN}$  or offset from the cometocentric rest velocity of  $0 \text{ km s}^{-1}$ .

Table 4 lists the molecular species that were searched for toward Comets Hale-Bopp and LINEAR at or near the cometocentric velocity ( $0 \text{ km s}^{-1}$ ). Least square Gaussian fits were made for each spectral line in order to obtain the peak intensities and line-widths for the

detected transitions. For those transitions not detected, the  $1\sigma$  rms noise level is given. The spectroscopic parameters used in determining the column densities and production rates are found in Table 3 and the formalism for calculating column densities and production rates is described in §4.1.

## 4. ANALYSIS AND DISCUSSION

### 4.1. EXCITATION, ABUNDANCES AND PRODUCTION RATES

Determining the best temperature, column density, and production rates of cometary molecules are important because they are essential to understanding the formation of cometary species. This includes the role of grains in molecule formation, the relative impact of warm versus cold gas phase chemistry, or the importance of photodissociation in the production of daughter species in the coma. In order to determine the temperatures and column densities of the region of the coma that contains the  $\text{CH}_3\text{OH}$  and  $\text{CH}_3\text{CN}$  emission, we assume that each region has uniform physical conditions, that the populations of the energy levels can be characterized by a Boltzmann distribution and finally, that the emission is optically thin. The rotational temperature diagram method was not employed for this analysis because even small errors in the intensities and widths of inherently weak spectral lines can cause large errors in determining the temperature and total column density (see e.g. Snyder et al. 2005). The complete formalism for these calculations using the BIMA array data can be found in Remijan et al. (2006) and for the 12m data, in Milam et al. (2006).

Figure 1 shows the results of the model fit (blue trace) applied to the  $\text{CH}_3\text{OH}$  BIMA array data. The array data are well fit by an excitation temperature of  $T_{ex}=105\pm5$  K and a total beam-averaged column density of  $N_T=9\pm1\times10^{14}\text{ cm}^{-2}$  assuming that the  $\text{CH}_3\text{OH}$  emission is extended beyond the  $10.''33\times8.''46$  average synthesized beam of the BIMA array (i.e. the beam filling factor,  $f=1$ ). Similarly, Figure 2 shows the results of the model fit applied to the  $\text{CH}_3\text{OH}$  ARO 12m data with the same excitation temperature and a slightly lower column density of  $N_T=2.4\pm0.3\times10^{14}\text{ cm}^{-2}$ . The average total column density from these two facilities is  $N_T=5.7\pm0.7\times10^{14}\text{ cm}^{-2}$ . As the figure shows, the modeling reproduces the observations. Assuming  $\text{CH}_3\text{OH}$  is a parent species, production rates were determined from a Monte Carlo model for a nuclear source (see Combi & Smyth, 1988). This model traces the trajectories of molecules, within the telescope beam, ejected from the comet surface. The observed column density is then matched for an output molecular production rate,  $Q$  ( $\text{s}^{-1}$ ). Input parameters include the lifetime of the molecule, from Huebner et al. (1992), scaled by  $R_h^2$ , the outflow velocity, telescope beam size, and the observed column density. Assuming a nuclear origin for  $\text{CH}_3\text{OH}$  and using this Monte Carlo model, we find

an average  $\text{CH}_3\text{OH}$  production rate from both instruments of  $Q(\text{CH}_3\text{OH}) \sim 1.3 \times 10^{29} \text{ s}^{-1}$  or  $Q(\text{CH}_3\text{OH})/Q(\text{H}_2\text{O}) \sim 1.3\%$  at  $\sim 1 \text{ AU}$ . This production rate ratio assumes a  $Q(\text{H}_2\text{O}) = 10^{31} \text{ s}^{-1}$  (Crovisier et al. 2004).

In Figure 2, there is a slight discrepancy between the observed intensities and model predictions for the  $\text{CH}_3\text{OH}$  lines at 151.86 GHz. The model predicts a higher line intensity than observed and the model underestimates the line intensity at 148.11 GHz and 145.76 GHz. However, given the S/N ratio of all the passbands where these lines are observed, the model does a very good job in predicting the expected line intensity of each  $\text{CH}_3\text{OH}$  transition observed with the 12m telescope. The same can be said for the array data. The only discrepancy is the 96.7445 GHz,  $J(K_a, K_c) = 2(0, 2) - 1(0, 1)$  E  $\text{CH}_3\text{OH}$  transition (Figure 1); the intensity is somewhat underestimated by our model fit.

Figure 4 shows the best model fit to the  $J(K) = 8(K) - 7(K)$  ( $K=0$  through 6) transitions of methyl cyanide ( $\text{CH}_3\text{CN}$ ) toward Comet Hale-Bopp. Once again, the blue trace shows the model predictions for the  $\text{CH}_3\text{CN}$  data which is best fit by an excitation temperature,  $T_{\text{ex}} = 200 \pm 10 \text{ K}$  and a total beam-averaged column density,  $N_T = 2.6 \pm 0.3 \times 10^{12} \text{ cm}^{-2}$ . In this case, the predicted  $K = 7$  line intensity is below the  $1 \sigma$  detection limit, which indicates that the emission feature near the  $K = 7$  rest frequency may not be real. Assuming a nuclear origin for  $\text{CH}_3\text{CN}$  and using a Monte Carlo model, we find a production rate of  $Q(\text{CH}_3\text{CN}) \sim 1.7 \times 10^{27} \text{ s}^{-1}$  or  $Q(\text{CH}_3\text{CN})/Q(\text{H}_2\text{O}) \sim 0.017\%$  at  $\sim 1 \text{ AU}$ . This production rate is similar to what Biver et al. (1997) found,  $\sim 10^{27} \text{ s}^{-1}$  at 1 AU, in their study.

These 12 m data overlap in frequency with the  $(\text{CH}_2\text{OH})_2$  IRAM 30m study of Crovisier et al. (2004). In the IRAM dataset, the claimed detection of the  $J(K_a, K_c, v) = 15(7, 9, 0) - 14(7, 8, 1)$  and  $15(7, 8, 0) - 14(7, 7, 1)$  transitions at 147.13 GHz are nearly coincident in frequency and show up as one feature given the spectral resolution. Moreover, the  $(\text{CH}_2\text{OH})_2$  transitions have an overall line intensity equal to that of the  $J(K) = 8(4) - 7(4)$  transition of  $\text{CH}_3\text{CN}$  detected with the IRAM 30m. From the ARO 12m data, we identify the same spectral features of  $\text{CH}_3\text{CN}$  but do not detect any emission from the two transitions of  $(\text{CH}_2\text{OH})_2$  below the  $1\sigma$  limit. From the  $\text{CH}_3\text{CN}$ ,  $\text{CH}_3\text{OH}$  and  $(\text{CH}_2\text{OH})_2$  12m data, it is clear we are probing different physical environments in the coma of Comet Hale-Bopp. A discussion of the distribution of these molecular species is in §4.2.

Figure 3 shows the best model fit (blue trace) to the cluster of E-type transitions of  $\text{CH}_3\text{OH}$  centered around 157.26 GHz toward Comet LINEAR with the ARO 12m telescope. There have been very few molecular line observations toward Comet LINEAR. The most complete study of molecular species toward this object was by Remijan et al. (2006) using the BIMA array. These authors detected the  $J(K_a, K_c) = 3(1, 3) - 4(0, 4)$  A<sup>+</sup> tran-



sition of CH<sub>3</sub>OH with a synthesized beam size of 22.''3 × 16.''9. Using the proposed excitation temperature of 115 K (DiSanti et al. 2004; Magee-Sauer et al. 2004; Küppers et al. 2004), Remijan et al. determined a total beam-averaged column density of CH<sub>3</sub>OH of  $N_T = 1.4 \pm 0.3 \times 10^{14} \text{ cm}^{-2}$ . However, as shown in figure 3, the 12m CH<sub>3</sub>OH data are best fit by an excitation temperature of  $T_{ex} = 35 \pm 5 \text{ K}$  and a total beam-averaged column density of  $N_T = 2.2 \pm 0.3 \times 10^{13} \text{ cm}^{-2}$  (blue trace), implying a production rate of  $Q(\text{CH}_3\text{OH}) \sim 2.0 \times 10^{27} \text{ s}^{-1}$  or  $Q(\text{CH}_3\text{OH})/Q(\text{H}_2\text{O}) \sim 1.5\%$  at 0.3 AU. This production rate ratio assumes a  $Q(\text{H}_2\text{O}) = 1.3 \times 10^{29} \text{ s}^{-1}$  (Lecacheux et al. 2004). To reconcile the differing column density determined by Remijan et al. (2006), we used the best model fit parameters of temperature and column density from the 12m data to predict the line intensity of the  $J(K_a, K_c) = 3(1,3) - 4(0,4) \text{ A}^+$  transition detected by the BIMA array. Figure 5 shows the result of this analysis (5(a) shows the hanning smoothed data and 5(b), the raw data as shown in figure 1 of Remijan et al. (2006)). The fit is excellent. From using the ARO data it is quite clear that the assumption of an excitation temperature of  $T_{ex} = 115 \text{ K}$  for CH<sub>3</sub>OH was incorrect and the determined column density of CH<sub>3</sub>OH toward Comet LINEAR was therefore overestimated by almost an order of magnitude.

#### 4.2. DISTRIBUTION OF MOLECULAR SPECIES

We present two complementary sets of data from Comet Hale-Bopp that give great insights into the distribution of CH<sub>3</sub>OH, CH<sub>3</sub>CN and (CH<sub>2</sub>OH)<sub>2</sub>. First, it is quite clear from the data presented in Figures 1 and 2 that despite the drastic change in the telescope beam sizes between the array and the 12m, we are still sampling a region of the coma that is thermalized to  $\sim 105 \text{ K}$ . The ratio of areas subtended by the 12m beam, compared to the BIMA array synthesized beam, is  $\sim 21:1$  which corresponds to a change in the physical sampled size scale from  $D \sim 40000 \text{ km}$  to  $D \sim 8500 \text{ km}$ . A direct comparison of the column densities from the 12m and BIMA array suggest an enhancement of the CH<sub>3</sub>OH abundance at smaller coma radii. Furthermore, Column 5 in table 3 lists the Einstein A coefficients for each transition of CH<sub>3</sub>OH, CH<sub>3</sub>CN and (CH<sub>2</sub>OH)<sub>2</sub>. Assuming a collision cross section of  $\sim 10^{-15} \text{ cm}^2$  and a temperature of 105 K, the calculated critical densities of the detected CH<sub>3</sub>OH transitions range from  $(0.7 - 3.2) \times 10^5 \text{ cm}^{-3}$ . Our observations encompass a region with a H<sub>2</sub>O density of  $\sim 10^{(5.7 - 7.5)} \text{ cm}^{-3}$  (Lovell et al. 2004). Therefore, there is sufficient collisional excitation to populate the CH<sub>3</sub>OH levels, and our observations are sampling molecular abundances and not excitation effects.

Figure 6(a) once again shows the distribution of the  $J(K_a, K_c) = 3(1,3) - 4(0,4) \text{ A}^+$  transition of CH<sub>3</sub>OH around Comet Hale-Bopp. Figure 6(b) is a model fit to the data shown in (a).

The model was generated assuming a spherical Haser model of parent species sublimating off the comet’s nucleus. From the data in (a), the scale length of the distribution of  $\text{CH}_3\text{OH}$  around the nucleus is measured to be  $r \sim 10''$ . Using this scale length and the MIRIAD task IMGEN, a Haser model distribution of  $\text{CH}_3\text{OH}$  was generated which was then convolved with the synthesized beam of the BIMA array (shown at the bottom left of each panel in figure 6). The residuals obtained by subtracting the model from the data are shown in figure 6(c). While it appears that there may be a more extended distribution of  $\text{CH}_3\text{OH}$  detected by the BIMA array based on the residual data, it is important to note that the contour levels shown in (a) and (b) are 3, 4, 5 and 6  $\sigma$  ( $\sigma = 0.05 \text{ Jy beam}^{-1}$ ), whereas the data shown in (c) are 1 and 1.5  $\sigma$ . Although there is some indirect evidence for an extended distribution of  $\text{CH}_3\text{OH}$  with  $D = 40000 \text{ km}$  from the 12 m detections of  $\text{CH}_3\text{OH}$ , the data presented in (c) indicate that any extended emission is completely resolved out by the array. The array would be sensitive to extended emission of  $\text{CH}_3\text{OH}$  in the outer coma only if the distribution was “clumpy”, as is seen in  $\text{H}_2\text{CO}$  (Milam et al. 2006).

It appears that the  $\text{CH}_3\text{CN}$  is tracing higher temperature and higher density gas than  $\text{CH}_3\text{OH}$ . Because  $\text{CH}_3\text{CN}$  has a larger dipole moment than  $\text{CH}_3\text{OH}$ , its measured excitation should be lower, given identical conditions. However, if the overall distribution of  $\text{CH}_3\text{CN}$  is closer to the nucleus than  $\text{CH}_3\text{OH}$ , we would expect to measure a higher excitation temperature (it is well known that the temperature of the coma increases with decreasing coma radii (Biver et al. 1999)). This distribution would also imply that  $\text{CH}_3\text{CN}$  is a parent species (§4.3). Given the difference in beam sizes between the 12m and 30m telescopes, we can get an estimate of the size of the emitting region based on the relative beam sizes using the beam filling factor in the expression for column density. Comparing the relative line intensities between the  $K=3$  and 4 transitions of  $\text{CH}_3\text{CN}$  from the IRAM 30m data and what is measured from the 12m, the 30m emission features from  $\text{CH}_3\text{CN}$  are  $\sim 5\text{-}10\times$  stronger than what is observed from the 12m. This difference implies either 1) an enhancement of the  $\text{CH}_3\text{CN}$  column density at smaller coma radii or 2) the excitation of the transitions we observed of  $\text{CH}_3\text{CN}$  takes place at a slightly smaller radii where the density is higher and the measurements taken with the 12m are suffering from some beam dilution. Assuming the  $\text{H}_2\text{O}$  density profile of Lovell et al. (2004), the maximum coma radius that lies below the  $\text{CH}_3\text{CN}$  critical density range of  $(1.2\text{-}5.3) \times 10^6 \text{ cm}^{-3}$  is  $\sim 10000 \text{ km}$ . This explains why the 30m  $\text{CH}_3\text{CN}$  line strengths are higher than those from the 12m. Finally, from the non-detection of  $(\text{CH}_2\text{OH})_2$  in the 12m observations, it is also apparent that the distribution of  $(\text{CH}_2\text{OH})_2$  must also be compact in the cometary coma. Assuming the detected transition line strength of  $\sim 0.09 \text{ K}$  in the 30m spectrum is from  $(\text{CH}_2\text{OH})_2$  and a  $1\sigma$  line intensity of  $\sim 0.01 \text{ K}$  in the 12m passband, the emission from  $(\text{CH}_2\text{OH})_2$  must be on the order of  $D < 9''$  corresponding to a physical size of  $D < 8500 \text{ km}$ . High sensitivity, high resolution interferometer observations

are necessary to confirm this distribution.

### 4.3. FORMATION OF COMETARY METHANOL AND OTHER MOLECULAR SPECIES

From the high resolution methanol observations of the BIMA array, it is clear that the  $\text{CH}_3\text{OH}$  is either sublimating directly off the cometary ices contained in the nucleus or is formed very deep in cometary coma. If  $\text{CH}_3\text{OH}$  originates in the ices, this molecule may be a remnant from the formation of the presolar nebula and hence the interstellar medium. Currently, there are two accepted formation pathways to the interstellar production of  $\text{CH}_3\text{OH}$ , including the radiative association of  $\text{CH}_3^+ + \text{H}_2\text{O} \rightarrow \text{CH}_3\text{OH}_2^+$ , followed by recombination with an electron to produce  $\text{CH}_3\text{OH}$  and  $\text{H}$  (Herbst, 1985). Grain surface reactions that involve the repeated hydrogenation of  $\text{CO} \rightarrow \text{H} + \text{CO} \rightarrow \text{HCO} + \text{H} \rightarrow \text{HCHO} \rightarrow \text{HCHOH}$  are thought to eventually lead to  $\text{CH}_3\text{OH}$  (Hiraoka et al. 1994). Our observations show there is no significant enhancement in the production of  $\text{CH}_3\text{OH}$  in the outer coma as the comet enters the inner solar system.

The same argument can be applied to  $\text{CH}_3\text{CN}$ . The accepted route to the formation of  $\text{CH}_3\text{CN}$  in interstellar environments is  $\text{CH}_3^+ + \text{HCN}$ , a collision complex is formed that equilibrates to  $\text{CH}_3\text{CNH}^+ + \nu$  (Herbst, 1985); then  $\text{CH}_3\text{CNH}^+$  combines with an electron to form  $\text{CH}_3\text{CN} + \text{H}$ . Our observations of  $\text{CH}_3\text{CN}$  show that it is present close to the cometary nucleus, indicating direct sublimation off cometary ices. However, the excitation of the transitions we observed of  $\text{CH}_3\text{CN}$  takes place at a smaller radii where the density is higher, and this molecule may be present as well at larger radii. However, the true spatial scale and scale length of  $\text{CH}_3\text{CN}$  needs to be verified by interferometric observations.

Finally, the non-detection of  $(\text{CH}_2\text{OH})_2$  with the ARO 12m gives insight into the formation of  $(\text{CH}_2\text{OH})_2$  as well as the possibility of detecting  $\text{CH}_2\text{OHCHO}$ . If the transition detected by the 30m is indeed from cometary  $(\text{CH}_2\text{OH})_2$ , in §4.2, we found the predicted distribution of  $(\text{CH}_2\text{OH})_2$  toward Comet Hale-Bopp was calculated to be  $D < 9''$  ( $< 8500$  km), again suggesting direct sublimation off cometary ices or an enhanced production in the inner coma. Presumably, as with the formation of  $\text{CH}_3\text{OH}$  and  $\text{CH}_3\text{CN}$  in interstellar environments,  $(\text{CH}_2\text{OH})_2$  would be formed in the ISM and then seeded into cometary ices. Currently, there is no accepted gas phase interstellar formation mechanism that can lead to the production of  $(\text{CH}_2\text{OH})_2$ . However, there are several formation pathways using surface chemistry which may occur on icy grain mantles. For example, to form  $(\text{CH}_2\text{OH})_2$  and  $\text{CH}_2\text{OHCHO}$ , formaldehyde ( $\text{H}_2\text{CO}$ ) produces  $\text{CH}_2\text{OHCHO}$  in an aqueous Formose reaction, which can then be hydrogenated to form  $(\text{CH}_2\text{OH})_2$  (e.g., see Walker 1975). Charnley (2001)

predicts that  $(\text{CH}_2\text{OH})_2$  and  $\text{CH}_2\text{OHCHO}$  could be formed by direct hydrogenation reactions, starting from ketene ( $\text{CH}_2\text{CO}$ ) on grain surfaces. Finally, Hudson & Moore (2000) showed that proton irradiated  $\text{CH}_3\text{OH}$  on icy interstellar grain mantles can lead to the formation of  $(\text{CH}_2\text{OH})_2$ . Thus, there appear to be several ways to form and embed  $(\text{CH}_2\text{OH})_2$  into cometary ices.

## 5. CONCLUSIONS

We presented an interferometric and single dish study of cometary molecules toward comets C/1995 O1 (Hale-Bopp) and C/2002 T7 (LINEAR) using the Berkeley-Illinois-Maryland Association (BIMA) interferometer at 3 mm and the Arizona Radio Observatory (ARO) 12m telescope at 2 mm. The overall conclusions from our analysis of these data are:

1. The  $\text{CH}_3\text{OH}$  Hale-Bopp data are well fit by an excitation temperature of  $T_{ex}=105\pm5$  K and a total beam-averaged column density of  $N_T=5.7 \pm 0.7 \times 10^{14} \text{ cm}^{-2}$ . Assuming a nuclear origin for  $\text{CH}_3\text{OH}$  and using a Monte Carlo model, we find an average  $\text{CH}_3\text{OH}$  production rate from both instruments of  $Q(\text{CH}_3\text{OH})\sim 1.3\times 10^{29} \text{ s}^{-1}$  or  $Q(\text{CH}_3\text{OH})/Q(\text{H}_2\text{O})\sim 1.3\%$  at  $\sim 1$  AU.
2. The  $\text{CH}_3\text{OH}$  ARO 12m LINEAR data centered around 157.26 GHz are best fit by an excitation temperature of  $T_{ex}=35\pm5$  K and a total beam-averaged column density of  $N_T=2.2\pm 0.3\times 10^{13} \text{ cm}^{-2}$  and thus, a production rate  $Q(\text{CH}_3\text{OH})\sim 2.0\times 10^{27} \text{ s}^{-1}$  or  $Q(\text{CH}_3\text{OH})/Q(\text{H}_2\text{O})=1.5\%$  at 0.3 AU.
3. From the combination of the single-dish and aperture synthesis observations of  $\text{CH}_3\text{OH}$ , we find the distribution of  $\text{CH}_3\text{OH}$  toward Comet Hale-Bopp is well described by a spherical outflow with an increase in column density closer to the cometary nucleus. The data presented in the array images show no evidence of significant enhanced production of  $\text{CH}_3\text{OH}$  in the extended coma or from jets as any extended emission is completely resolved out by the array.
4. The  $\text{CH}_3\text{CN}$  12m Hale-Bopp data is best fit by an excitation temperature,  $T_{ex}=200\pm 10$  K and a total beam-averaged column density,  $N_T=2.6\pm 0.3\times 10^{12} \text{ cm}^{-2}$ . Assuming a nuclear origin for  $\text{CH}_3\text{CN}$  and using a Monte Carlo model, we find an average  $\text{CH}_3\text{CN}$  production rate of  $Q(\text{CH}_3\text{CN})\sim 1.7\times 10^{27} \text{ s}^{-1}$  or  $Q(\text{CH}_3\text{CN})/Q(\text{H}_2\text{O})\sim 0.017\%$  at  $\sim 1$  AU. A comparison between the single-dish observations from the ARO 12m and the IRAM 30m of  $\text{CH}_3\text{CN}$  suggest that the ARO observations are beam diluted. The excitation of the transitions observed of  $\text{CH}_3\text{CN}$  takes place at a smaller radii where the density is higher and suggest a nuclear origin of  $\text{CH}_3\text{CN}$ .

5. The non-detection of a previously claimed transition of cometary  $(\text{CH}_2\text{OH})_2$  toward Comet Hale-Bopp with the ARO 12m telescope indicates a compact distribution of emission on the order of  $<9''$  ( $<8500$  km). This supports the hypothesis that the cometary production of  $(\text{CH}_2\text{OH})_2$  is direct sublimation off cometary ices from the nucleus.

We thank D. K. Yeomans for ephemerides assistance and G. Engargiola, T. Helfer, W. Hoffman, R. L. Plambeck, and M. W. Pound for invaluable technical contributions. We also thank an anonymous referee for a favorable review of this work and whose comments and suggestions provided additional clarity to this manuscript. This material is based on work supported by the National Aeronautics and Space Administration through the NASA Astrobiology Institute under Cooperative Agreement CAN-02-OSS-02 issued through the Office of Space Science. S. N. M. would like to thank the Phoenix Chapter of ARCS, specifically Mrs. Scott L. Libby, Jr. endowment, for partial funding. This work was partially funded by NASA NAG5-4292, NAG5-4080, NAG5-8708, and NGT5-0083; NSF AST 96-13998, AST96-13999, AST96-13716, AST96-15608, and AST99-81363; and the Universities of Illinois, Maryland, and California, Berkeley. M. W. was funded by NSF AST 9625360, AST 9796263, and AST 0098583 and NASA NAG5-4349.

## REFERENCES

- Araya, E., Hofner, P., Kurtz, S., Bronfman, L., & DeDeo, S. 2005, *ApJS*, 157, 279
- Biver, N., et al. 1997, *Earth, Moon & Planets*, 78, 5
- Biver, N., et al. 1999, *AJ*, 118, 1850
- Biver, N., et al. 2002, *Earth, Moon, and Planets*, 90, 1, 5
- Bockelée-Morvan, D., Crovisier, J., Despois, D., Forveille, T., Gerard, E., Schraml, J., & Thum, C. 1987, *A&A*, 180, 253
- Bonev et al. 2008, arXiv: 0804.4673v1
- Charnley, S. B. 2001, in *The Bridge between the Big Bang and Biology*, ed. F. Giovannelli (Special Vol.; Rome: Consiglio Naz. Ric.), 139
- Charnley, S. B. & Rodgers, S. D. 2008, *Space Science Reviews*, Online First
- Christen. D., & Müller, H. S. P. 2003, *Phys. Chem.*, 5, 3600

- Colom, P., Despois, D., Bockelée-Morvan, D., Crovisier, J., & Paubert, G. 1990, In Southwest Research Inst., Workshop on Observations of Recent Comets, 80
- Combi, M. R., & Smyth, W. H. 1988, *ApJ*, 327, 1026
- Crovisier, J., Bockelée-Morvan, D., Biver, N., Colom, P., Despois, D., & Lis, D. 2004, *A&A*, 418, L35
- DiSanti, M. A., Reuter, D. C., Mumma, M. J., Dello Russo, N., Magee-Sauer, K., Gibb, E. L., Bonev, B., & Anderson, W. M. 2004, *BAAS*, 36, 1122
- Herbst, E. 1985, *ApJ*, 291, 226
- Hiraoka, K., Ohashi, N., Kihara, Y., Yamamoto, K., Sato, T., & Yamashita, A. 1994, *Chem. Phys. Lett.*, 229, 408
- Hofner, P., Kurtz, S., Churchwell, E., Walmsley, C. M., & Cesaroni, R. 1996, *ApJ*, 460, 359
- Hudson, R. L. & Moore, M. H. 2000, *Icarus*, 145, 661
- Hudson, R. L., Moore, M. H., & Cook, A. M. 2005, *Adv. in Space Research*, 36, 183
- Huebner, W. F., Keady, J. J., & Lyon, S. P. 1992, *Ap&SS*, 195, 291
- Küppers, M., Hartogh, P., & Villanueva, G. 2004, *BAAS* 36, 1125
- Lecacheux, A., Biver, N., Crovisier, J., & Bockelée-Morvan, D. 2004, *IAU Circ.*, 8304, 2
- Lovell, A. J., Kallivayalil, N., Schloerb, F. P., Combi, M. R., Hansen, K. C., & Gombosi, T. I. 2004, *ApJ*, 613, 615
- Magee-Sauer, K., Mumma, M. J., DiSanti, M. A., Russo, N. D., & Rettig, T. W. 1999, *Icarus*, 142, 498
- Milam, S. N., et al. 2006, *ApJ*, 649, 1169
- Müller, H. S. P., Schloder, F., Stutzki, J., & Winnenwischer, G. 2005, *J. Mol. Struct.*, 742, 215
- Mumma, et al. 2003, *AdSpRev*, 31, 2563
- Remijan, A., Sutton, E. C., Snyder, L. E., Friedel, D. N., Liu, S.-Y., & Pei, C.-C. 2005, *ApJ*, 606, 917
- Remijan, A. J., et al. 2006, *ApJ*, 643, 567

- Remijan, A. J. & Markwick-Kemper, A. J. 2008, BAAS, 39, 963
- Sault, R. J., Teuben, P. J., & Wright, M. C. H. 1995, ASP Conf. Ser. 77: Astronomical Data
- Snyder, L. E., et al. 2005, ApJ, 619, 914
- Veal, J. M., Snyder, L. E., Wright, M., Woodney, L. M., Palmer, P., Forster, J. R., de Pater, I., A’Hearn, M. F., & Kuan, Y.-J. 2000, AJ, 119, 1498
- Walker, J. F. 1975, Formaldehyde (3d. ed.; Huntington: Robert E. Krieger), chap. 8
- Weissman, P. R. 1999, Space Science Reviews, 90, 301

Table 1. CH<sub>3</sub>OH Observational Parameters - BIMA array

Frequency (GHz)	Observation date	$\Delta$ (AU)	r (AU)	beam ("×")	chan rms (Jy beam <sup>-1</sup> )
96.741	1997 Mar 27	1.323	0.919	10.8×8.2	0.21
	1997 Mar 31	1.344	0.914	9.8×7.8	0.20
107.014	1997 Mar 26	1.320	0.921	19.3×6.8	0.43
	1997 Apr 02	1.359	0.914	11.7×6.6	0.15
	1997 Apr 03	1.367	0.915	16.0×6.4	0.30



Table 2. Observational Parameters - ARO 12m

Frequency (GHz)	Observation date	$\Delta$ (AU)	r (AU)	beam (")	D (km)	$\eta_c$	molecule
Comet Hale-Bopp							
145.766	1997 Mar 20.94	1.318	0.940	43	41105	0.76	CH <sub>3</sub> OH
147.105 <sup>a</sup>	1997 Mar 20.66	1.318	0.940	43	41105	0.76	CH <sub>3</sub> CN
148.112	1997 Mar 11.89	1.368	0.989	42	41672	0.76	CH <sub>3</sub> OH
150.142	1997 Mar 10.71	1.377	0.996	42	41946	0.75	CH <sub>3</sub> OH
151.860	1997 Mar 20.92	1.318	0.940	41	39193	0.74	CH <sub>3</sub> OH
157.049	1997 Mar 21.54	1.316	0.936	40	38179	0.72	CH <sub>3</sub> OH
Comet LINEAR							
157.261 <sup>b</sup>	2004 May 21.80	0.284	0.865	40	8239	0.72	CH <sub>3</sub> OH

<sup>a</sup>Average of observing frequencies between the  $K=7$  and  $K=0$  lines of CH<sub>3</sub>CN.

<sup>b</sup>Average of observing frequencies of CH<sub>3</sub>OH lines detected in the same spectral passband.

Table 3. Molecular Line Parameters

Molecule	Transition	Frequency (MHz)	$\langle S_{i,j}\mu^2 \rangle$ (Debye <sup>2</sup> )	$A_{i,j}$ (s <sup>-1</sup> )	E <sub>u</sub> (K)
CH <sub>3</sub> OH <sup>a</sup>	J(K <sub>a</sub> ,K <sub>c</sub> )=2(-1,2)-1(-1,1) E	96,739.363(3)	1.2	2.55×10 <sup>-6</sup>	12.6
	2(0,2)-1(0,1) A <sup>+</sup>	96,741.377(3)	1.6	3.41×10 <sup>-6</sup>	7.0
	2(0,2)-1(0,1) E	96,744.549(3)	1.6	3.41×10 <sup>-6</sup>	20.1
	2(1,1)-1(1,0) E	96,755.507(3)	1.2	2.62×10 <sup>-6</sup>	28.0
	3(1,3)-4(0,4) A <sup>+</sup>	107,013.770(13)	3.0	6.13×10 <sup>-6</sup>	28.4
	16(0,16)-16(-1,16) E	145,766.163(27)	7.0	7.60×10 <sup>-6</sup>	327.9
	15(0,15)-15(-1,15) E	148,111.919(24)	7.3	8.80×10 <sup>-6</sup>	290.9
	14(0,14)-14(-1,14) E	150,141.593(22)	7.5	10.2×10 <sup>-6</sup>	256.3
	13(0,13)-13(-1,13) E	151,860.170(20)	7.6	11.5×10 <sup>-6</sup>	223.9
	6(0,6)-6(-1,6) E	157,048.586(13)	5.7	1.96×10 <sup>-6</sup>	61.9
	4(0,4)-4(-1,4) E	157,246.041(14)	4.2	21.0×10 <sup>-6</sup>	36.4
	1(0,1)-1(-1,1) E	157,270.818(15)	1.5	22.1×10 <sup>-6</sup>	15.5
	3(0,3)-3(-1,3) E	157,272.320(14)	3.3	21.5×10 <sup>-6</sup>	27.1
	2(0,2)-2(-1,2) E	157,276.004(14)	2.4	21.8×10 <sup>-6</sup>	20.1
CH <sub>3</sub> CN <sup>a</sup>	J(K)=8(6)-7(6)	147,072.608(2)	53.2	0.58×10 <sup>-4</sup>	289.0
	8(5)-7(5)	147,103.741(1)	74.2	1.62×10 <sup>-4</sup>	210.5
	8(4)-7(4)	147,129.232(1)	91.3	1.99×10 <sup>-4</sup>	146.2
	8(3)-7(3)	147,149.068(1)	104.6	1.14×10 <sup>-4</sup>	96.1
	8(2)-7(2)	147,163.243(1)	114.1	2.49×10 <sup>-4</sup>	60.4
	8(1)-7(1)	147,171.750(1)	119.8	2.61×10 <sup>-4</sup>	38.9
	8(0)-7(0)	147,174.587(1)	121.7	2.66×10 <sup>-4</sup>	31.8
(CH <sub>2</sub> OH) <sub>2</sub> <sup>b</sup>	J(K <sub>a</sub> ,K <sub>c</sub> ,v)=15(7,9,0)-14(7,8,1)	147,131.814(36)	2.5	5.99×10 <sup>-5</sup>	83.1
	15(7,8,0)-14(7,7,1)	147,132.412(36)	2.7	5.99×10 <sup>-5</sup>	83.1

<sup>a</sup>Molecular line parameters of CH<sub>3</sub>OH and CH<sub>3</sub>CN taken from SLAIM at [www.splatalogue.net](http://www.splatalogue.net). Q<sub>r</sub>=1.2T<sub>r</sub><sup>3/2</sup> for CH<sub>3</sub>OH and Q<sub>r</sub>=3.9T<sub>r</sub><sup>3/2</sup> for CH<sub>3</sub>CN.

<sup>b</sup>Molecular line parameters of (CH<sub>2</sub>OH)<sub>2</sub> taken from CDMS (Müller et al. 2005). The energy levels are noted as J(K<sub>a</sub>,K<sub>c</sub>,v) where v is the quantum number associated with OH tunneling (Christen & Müller 2003).

Table 4. Comet Hale-Bopp and Comet LINEAR Molecular Line Identifications

Species	Telescope	$\nu$ (MHz)	Transition	$I_{line}$ <sup>a</sup>	$\Delta v$ (km s <sup>-1</sup> )	N <sub>T</sub> (cm <sup>-2</sup> )	Q <sub>P</sub> (s <sup>-1</sup> )	Q <sub>X</sub> /Q <sub>H<sub>2</sub>O</sub>
Comet Hale-Bopp								
CH <sub>3</sub> OH	BIMA	96,739.4	2(-1,2)-1(-1,1) E	0.31(5)	2.4(2)	9±1×10 <sup>14</sup>	1.1±0.3×10 <sup>29</sup>	~1.1×10 <sup>-2b</sup>
		96,741.4	2(0,2)-1(0,1) A <sup>+</sup>	0.52(5)	2.0(2)			
		96,744.5	2(0,2)-1(0,1) E	0.60(5)	2.1(2)			
		96,755.5	2(1,1)-1(1,0) E	0.29(5)	3.2(2)			
		107,013.8	3(1,3)-4(0,4) A <sup>+</sup>	1.12(5)	1.9(2)			
CH <sub>3</sub> OH	12m	145,766.2	16(0,16)-16(-1,16) E	0.03(2)	2.0(8)	2.4±0.3×10 <sup>14</sup>	1.5±0.3×10 <sup>29</sup>	~1.5×10 <sup>-2</sup>
		148,111.9	15(0,15)-15(-1,15) E	0.04(2)	3.0(8)			
		150,141.6	14(0,13)-14(-1,14) E	0.04(1)	1.9(8)			
		151,860.2	13(0,13)-13(-1,13) E	0.05(1)	2.5(8)			
		157,048.6	6(0,6)-6(-1,6) E	0.23(1)	2.4(8)			
			CH <sub>3</sub> OH	AVERAGE:	5.7±0.7×10 <sup>14</sup>			
CH <sub>3</sub> CN	12m	147,129.2	8(4)-7(4)	0.019(1)	1.6(8)	2.6±0.3×10 <sup>12</sup>	1.7±0.3×10 <sup>27</sup>	~1.7×10 <sup>-4</sup>
		147,149.0	8(3)-7(3)	0.054(1)	2.8(8)			
		147,163.2	8(2)-7(2)	0.034(1)	3.2(8)			
		147,171.7	8(1)-7(1)	0.049(1)	2.4(8)			
		147,174.5	8(0)-7(0)	0.051(1)	2.4(8)			
(CH <sub>2</sub> OH) <sub>2</sub>	12m	147,131.8	15(7,*,0)-14(7,*,0)	<0.01				
Comet T7/LINEAR								
CH <sub>3</sub> OH	12m	157,246.1	6(0,6)-6(-1,6) E	0.087(1)	1.9(10)	2.2±0.3×10 <sup>13</sup>	2.0±0.3×10 <sup>27</sup>	~1.5×10 <sup>-2c</sup>
		157,270.9	1(0,1)-1(-1,1) E	0.051(1)	1.9(10)			
		157,272.3	3(0,3)-3(-1,3) E	0.101(1)	1.9(10)			
		157,276.0	2(0,2)-2(-1,2) E	0.058(1)	1.9(10)			

<sup>a</sup>For the BIMA data,  $I_{line}$  represents  $\Delta I$  and are in units of Jy beam<sup>-1</sup>. For the 12m observations,  $I_{line}$  represents  $T_R^*$  in units of K.

<sup>b</sup>Comet Hale-Bopp:  $Q(H_2O)=10^{31} \text{ s}^{-1}$  (Crovisier et al. 2004)

<sup>c</sup>Comet T7/LINEAR:  $Q(H_2O)=1.3 \times 10^{29} \text{ s}^{-1}$  (Milam et al. 2006)

Fig. 1.—  $\text{CH}_3\text{OH}$  lines detected toward Comet Hale-Bopp with the BIMA array. (a) Emission contours from the  $2(0,2)\text{-}1(0,1)$  E transition of  $\text{CH}_3\text{OH}$  at 96.741 GHz. Contours indicate the location of the  $2(0,2)\text{-}1(0,1)$  E  $\text{CH}_3\text{OH}$  emission. The contour levels are -0.2, 0.4, 0.6, 0.8, 1.0, and 1.2 Jy beam $^{-1}$ . The synthesized beam of  $10''.3 \times 8''.5$  is indicated at the bottom left corner. (b)  $\text{CH}_3\text{OH}$  spectrum toward Comet Hale-Bopp (Hanning smoothed over three channels). The rms noise level is  $\sim 0.1$  Jy beam $^{-1}$  (indicated by the vertical bar at the left of the spectrum). The spectral line labels correspond to the rest frequency located at the top left of the spectral window for a velocity of 0 km s $^{-1}$ . The dashed line is centered on this velocity. The blue trace shows a model fit (see text). (c) Emission contours from the  $3(1,3)\text{-}4(0,4)$  A $^+$  transition of  $\text{CH}_3\text{OH}$  at 107.014 GHz. Contours indicate the location of the  $\text{CH}_3\text{OH}$  emission averaged between -2 km s $^{-1}$  and 2 km s $^{-1}$ . The contour levels are -0.05, 0.20, 0.30, 0.40, 0.50, and 0.60 Jy beam $^{-1}$ . The synthesized beam of  $10''.8 \times 7''.2$  is indicated at the bottom left corner. (d)  $\text{CH}_3\text{OH}$  spectrum toward Comet Hale-Bopp. The rms noise level is  $\sim 0.1$  Jy beam $^{-1}$  (indicated by the vertical bar at the left of the spectrum). The spectral line label is the same as in (b) and the blue trace shows a model fit (see text).

Fig. 2.—  $\text{CH}_3\text{OH}$  lines detected toward Comet Hale-Bopp with the 12m telescope. The backends employed for the presented observations were either filter banks with 500 kHz resolution or a millimeter autocorrelator (MAC) with a resolution of 781 kHz. The spectral line labels correspond to the rest frequency located at the top left of the spectral window for a velocity of 0 km s $^{-1}$  (dashed line). The blue traces show a model fit (see text).

Fig. 3.—  $\text{CH}_3\text{OH}$  lines detected toward Comet LINEAR with the 12m telescope. Spectral resolution is 500 kHz and the spectral line labels are similar to Figure 2. The blue traces show a model fit (see text).

Fig. 4.—  $\text{CH}_3\text{CN}$  lines detected toward Comet Hale-Bopp with the 12m telescope. Spectral resolution is 781 kHz and the spectral line labels are similar to Figure 2. The blue trace shows the model fit (see text).

Fig. 5.—  $\text{CH}_3\text{OH}$  transitions from Comet LINEAR and the model fit to the data (blue trace) from the BIMA array data.

Fig. 6.—  $\text{CH}_3\text{OH}$  Haser model fit to the BIMA array data. (a) The emission contours from the  $3(1,3)\text{-}4(0,4)$  A $^+$  transition of  $\text{CH}_3\text{OH}$  at 107.014 GHz. (b) The Haser model predictions to these data assuming a scale length of  $r \sim 10''$  and then convolved with the synthesized beam (shown at the bottom left). (c) The residuals obtained by subtracting the model from the data.

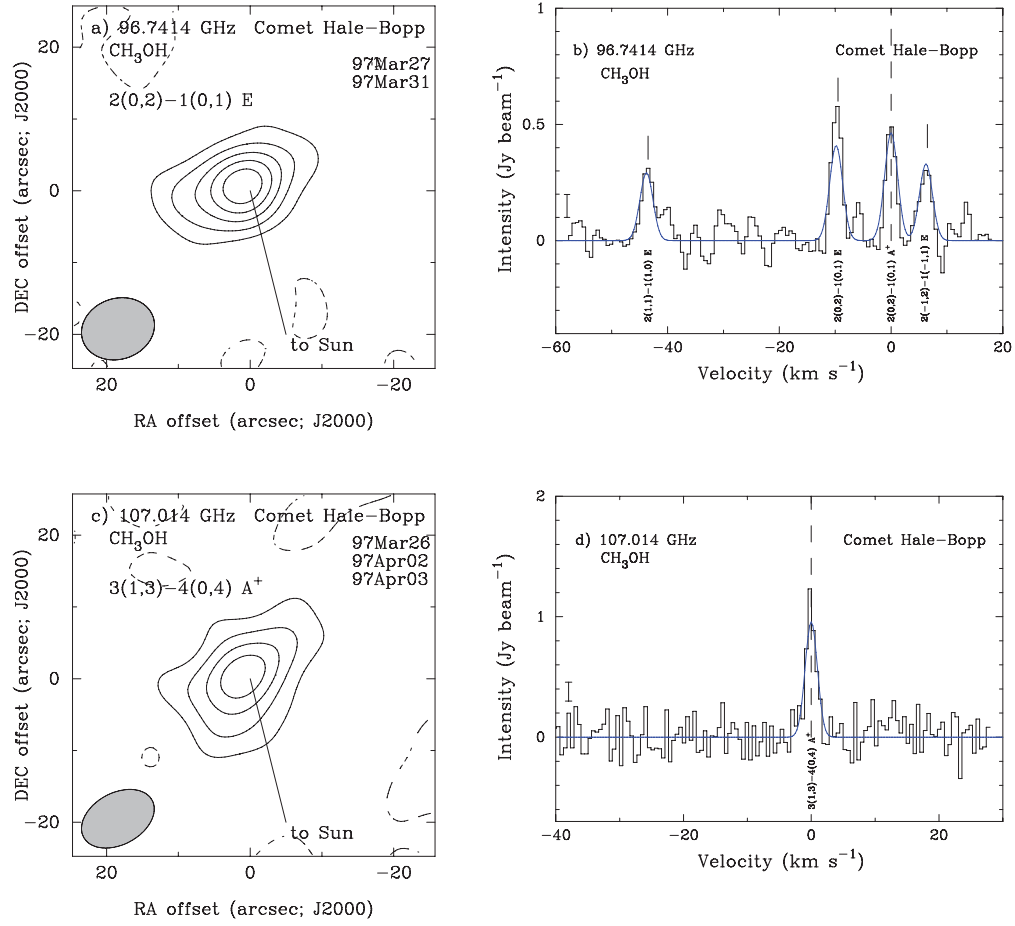


Figure 1.

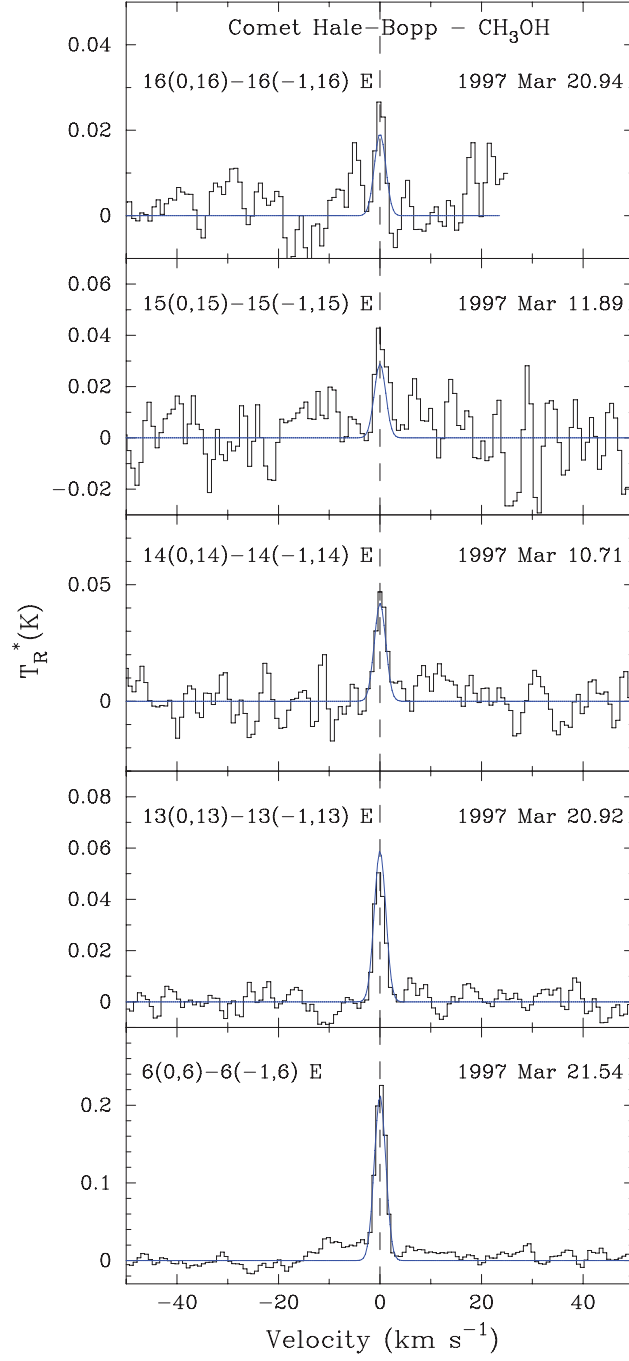


Figure 2.

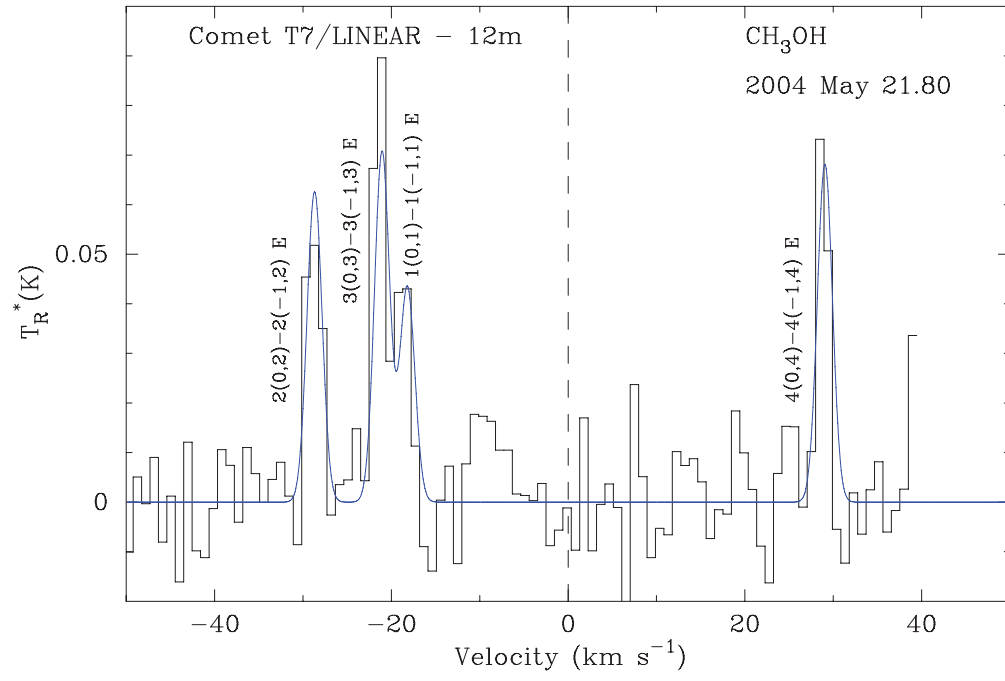


Figure 3.

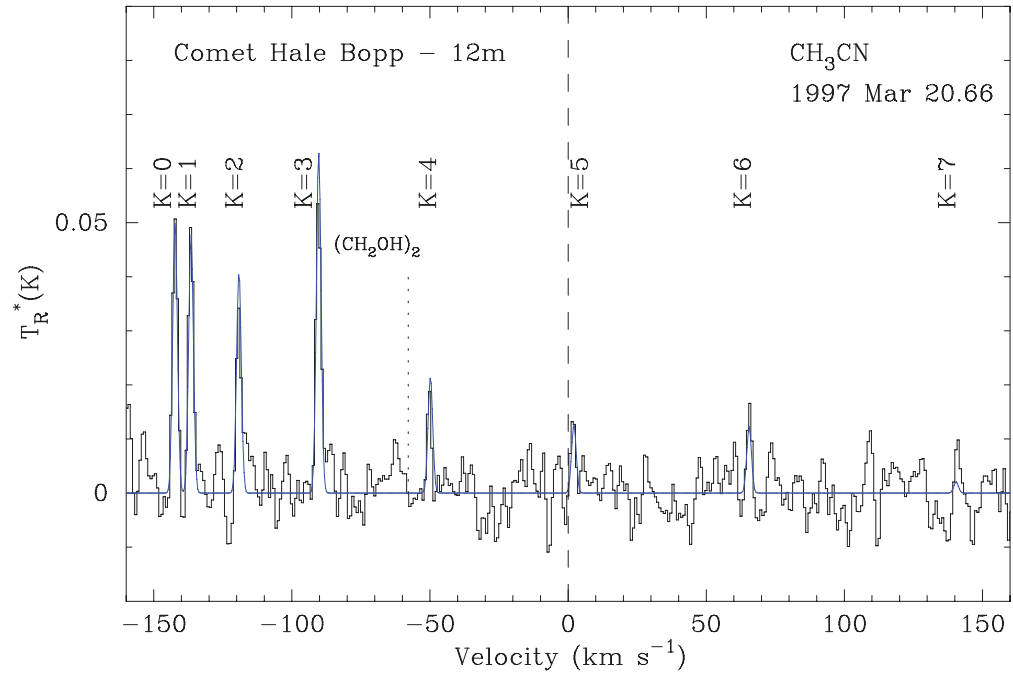


Figure 4.



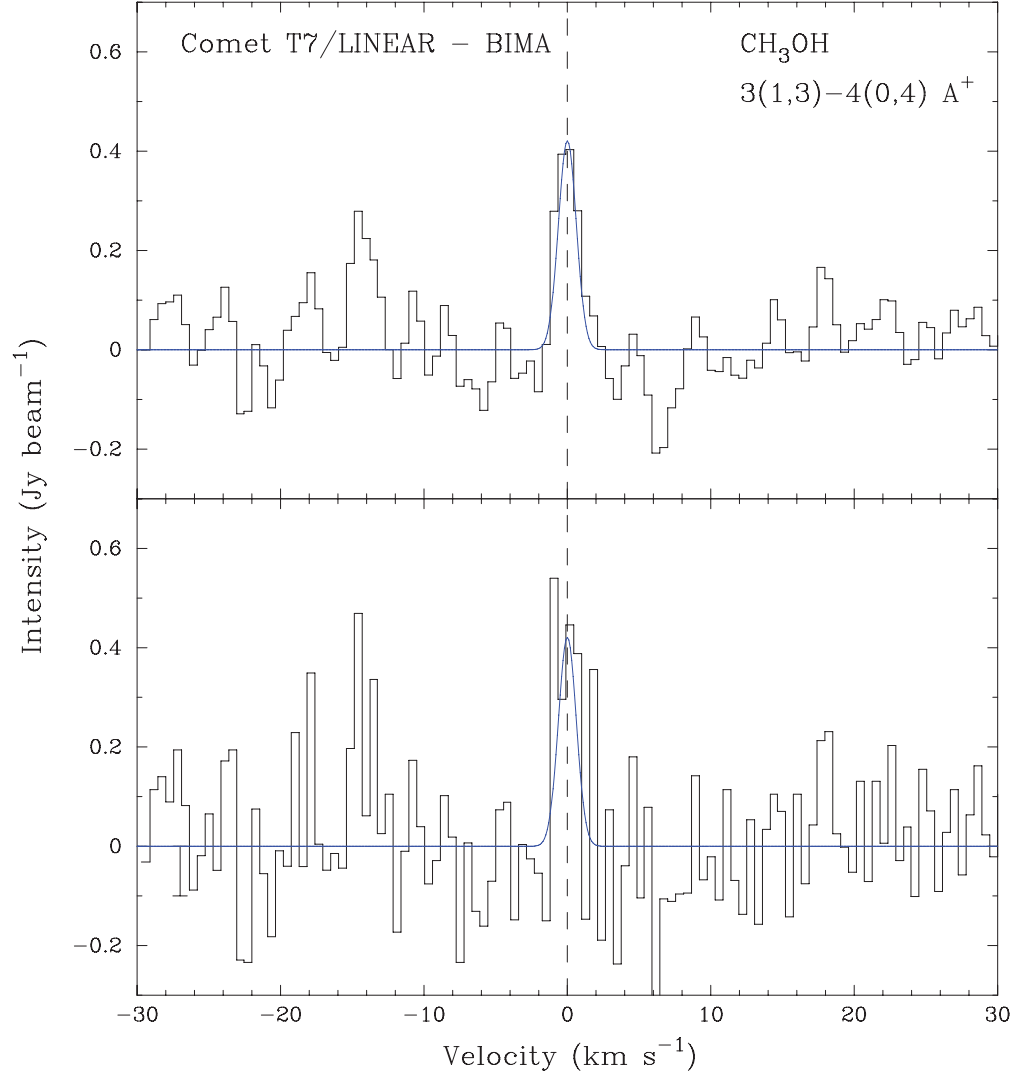


Figure 5.

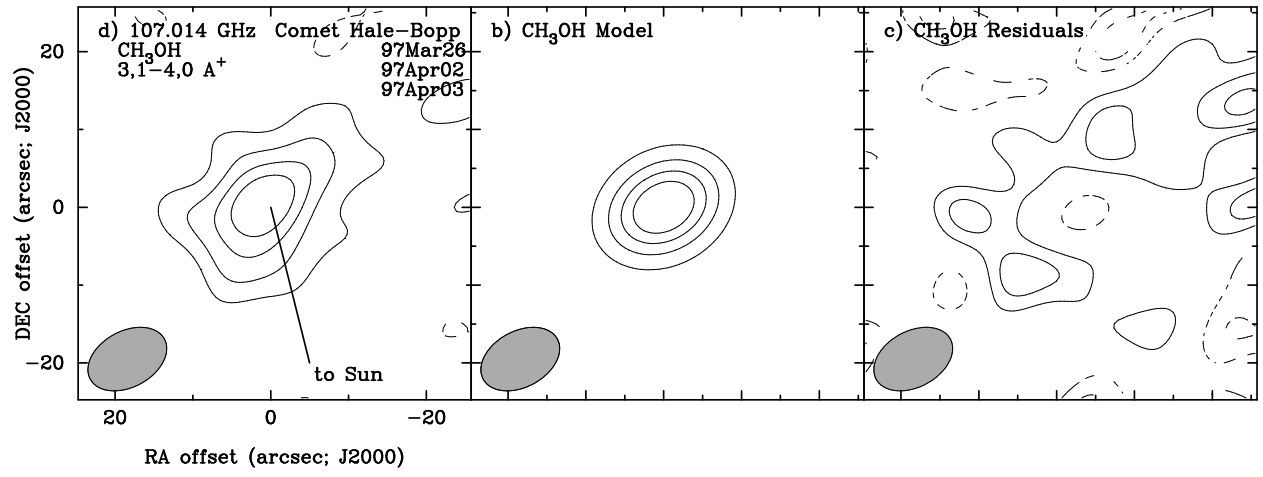


Figure 6.